Integration of seismic methods with reservoir simulation, Pikes Peak heavy-oil field, Saskatchewan

Y. Zou, L. R. Bentley, and L. R. Lines, University of Calgary, Alberta, Canada
D. Coombe, Computer Modeling Group, Calgary, Canada

Reservoir characterization is essential for providing optimal recovery from heavy-oil fields. The process of reservoir characterization is demonstrated for a steam injection project at Pikes Peak heavy oil field near Lloydminster, Saskatchewan, Canada. Geologic, geophysical and reservoir engineering data are used to improve the interpretation of reservoir conditions. There is ambiguity in modeling any of these data. However, in modeling all data sets in "cooperative inversion," ambiguity is decreased, thereby enhancing our knowledge of the reservoir. One of the main benefits of this oil-field modeling is that bypassed oil and steam fronts are effectively mapped.

Petroleum engineers use reservoir simulators to predict the evolution of pressure, temperature, and the saturation of water, oil, and gas during reservoir production. The results are then used to help make production decisions. Constructing a model requires that we define the geometry of the reservoir as well as model parameters such as porosity and permeability. The geometry and parameters are estimated using core, borehole logs, seismic surveys, and production tests. However, these parameters are never known with certainty because of scaling issues, uncertainty in test results, and the spatially sparse patterns of sampling. Consequently, production history matching suffers from nonuniqueness, and the initial simulation results typically compare poorly with measured pressure and production data. On the other hand, seismic data provide spatially dense information that can be related to the elastic properties of the subsurface and can be used to constrain the adjustment of reservoir model parameters. The additional model constraints imposed by seismic data provide a spatially dense sample and should reduce the level of nonuniqueness in the resultant estimated reservoir model parameter set. In this manner, rock physics provides a critical link for completing an integrated interpretation of seismic data and reservoir engineering data. Attempts to integrate geophysics and thermal reservoir simulation results have been reported (e.g., Jenkins et al., 1997), although the detailed procedures have generally not been published.

In the following case history, we present a practical procedure for using reservoir simulation results to generate synthetic time-lapse seismic responses. The procedure will then be applied to the Pikes Peak heavy oil field that has been undergoing thermal recovery operations for more than 20 years, and we will compare the synthetic results to the observed changes in the field. In the following sections, we will introduce the Pikes Peak Field, outline the seismic processing flow, describe the reservoir simulation model, summarize the rock physics procedure, present the seismic modeling, and finally discuss the integrated reservoir interpretation.

Pikes Peak heavy-oil field: Geologic setting and production history. The Pikes Peak heavy-oil field is 40 km east of Lloydminster, a town on the border between the provinces of Alberta and Saskatchewan, Canada (Figure 1). The Pikes Peak reservoir is located on an east-west structural high within an incised valley-fill channel complex that trends north south.

Editor's note: Y. Zou is now at Veritas.

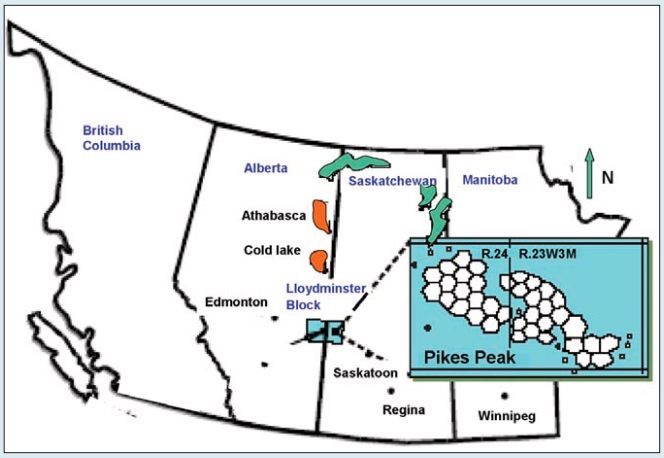

Figure 1. The location of Pikes Peak area (adapted from Wong et al., 2001).

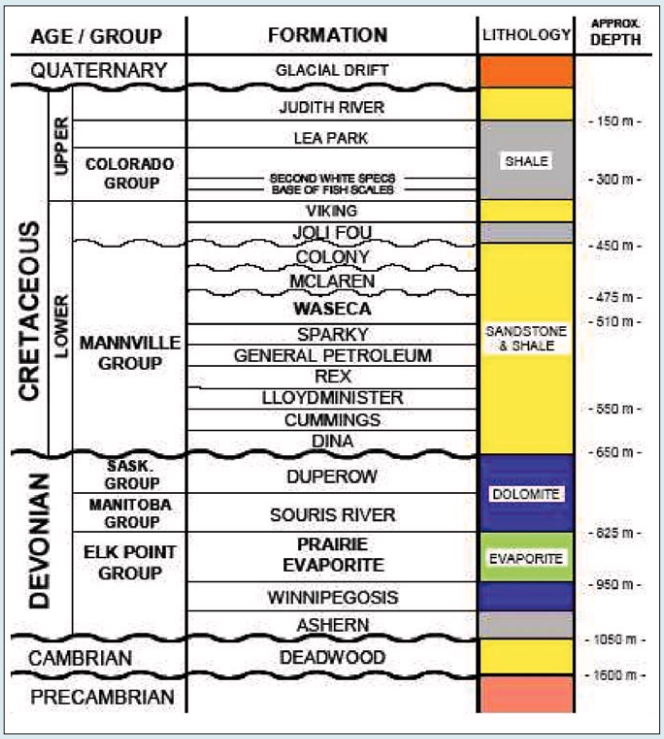

Figure 2. Pikes Peak stratigraphic chart (adapted from Watson, 2004).

Heavy oil is produced from an average depth of 500 m from the Waseca Formation of the Lower Cretaceous Mannville Group, as indicated in Figure 2. The Waseca Formation consists of a generally fining upward sequence with clean homogeneous unconsolidated quartzose sand at the base and sand-shale interbeds on top. The quality of the interbed unit decreases upward as a result of decreasing grain size and increasing clay content. The higher-quality lower interbeds often are in communication with the homogeneous sand unit and contribute to oil production. Locally, there are calcite-cemented tight streaks in the interval. The structural relief of the Mannville Group in the study area is complicated by dis-

solution of Middle Devonian Prairie Evaporite salt beds. The combination of the salt dissolution and differential compaction of the sand and shale in the Waseca interval are believed to have created the structural trap for the heavy oil. Typical properties for this reservoir include an oil saturation of 80%, oil gravity of 12° API, porosity of 34%, and permeability of 5000 md. The average sand thickness of the reservoir is 15 m. The best part of the reservoir is the structurally high central portion, which has the thickest homogenous sand (maximum 30 m), and has no bottom water. Most of the rest of the reservoir is underlain by bottom water.

Husky Energy has operated Pikes Peak Field for more than 25 years. After limited primary production, Husky started using cyclic steam stimulation (CSS) in 1981 with subsequent conversion to steam drive mostly in the western part of Pikes Peak in 1984. The good thermal efficiency of this project is reflected in the cumulative steam oil ratio (SOR) of 2.72 m^3/m^3 and current oil recoveries of up to 70% in the more mature steam-flooded areas. Forty percent, 6.56 $\times 10^6$ m^3, of the original oil-in-place had been recovered at the end of July 2001. Van Hulten (1984) provided a detailed geologic background for the Waseca Formation of Pikes Peak area. Sheppard et al. (1998) and Wong et al. (2001) reviewed the reservoir engineering history and the field development information.

Husky acquired 2D seismic surveys in 1991, forming grids of 29 north-south lines spaced every 100 m over the Pikes Peak area. As described by Watson et al. (2002), this vibroseis survey had 40 m source intervals, 20 m receiver group intervals, and had a CDP fold of 30. In March 2000, the University of Calgary and Husky acquired a repeat line on the eastern side of the field. This multicomponent survey had 20 m source interval, 20 m receiver group intervals and a CDP fold of 66. Table 1 outlines the seismic field parameters, and Table 2 outlines the reservoir properties.

The study area for this paper is in the eastern part of the Pikes Peak area. CSS started in 1983 in this part of the reservoir. Figure 3 shows a seismic line common to both the 1991 and 2000 surveys. The honeycomb shapes in Figure 3 are the seven-spot steam-drive well patterns. Most wells around the time-lapse seismic lines are CSS wells. This paper will focus on the profile indicated by the red line in Figure 3.

P-sonic and density logs from four wells, 1A15-6, D15-6, 3C8-6, and 1D2-6 were available for the study. Well 1A15-6 is the only well that has a shear wave sonic log. The density and gamma-ray logs clearly show the homogenous sand zone, and these were tied to the processed seismic sections. The original field data and survey files of the two time-lapse seismic 2D lines were available for this study. The detailed information will be described in the following section. An initial reservoir model and the production history files for the

Table 1. *Field parameters for 1991 and 2000 surveys.*

	1991 field parameters	2000 field parameters
Date	February 1991	March 2000
Sweep length	6 s	16 s
Sweep bandwidth	8–110 Hz	8–150 Hz
Antialias filter	8–110 HZ nonlinear	3–164 HZ nonlinear
Source array	3 vibs over 20 m	2 vibs over 20 m
Vibroseis drag length	10 m	No drag
Geophone frequency	14 Hz	10 Hz
Geophone interval	20 m	20 m
Source interval	40 m	20 m
Geophone array	9 over 20 m	6 over 20 m
Fold	30	66

Table 2. *Pikes Peak Waseca Channel homogeneous unit reservoir properties.*

Depth	~500 m
Initial temperature	18° C
Initial pressure	3350 KPa
Net pay (including lower interbeded zone)	5.7–27.5 m
Air permeability	4500–10 000 md
Porosity	0.34
Water saturation	0.08–0.22
Oil density	985 kg/m^3
Dead oil viscosity	25 000 mPa.s
Oil formation volume factor	1.025 m^3/m^3
Initial gas oil ratio (GOR)	14.5 m^3/m^3
Oil saturation	0.86

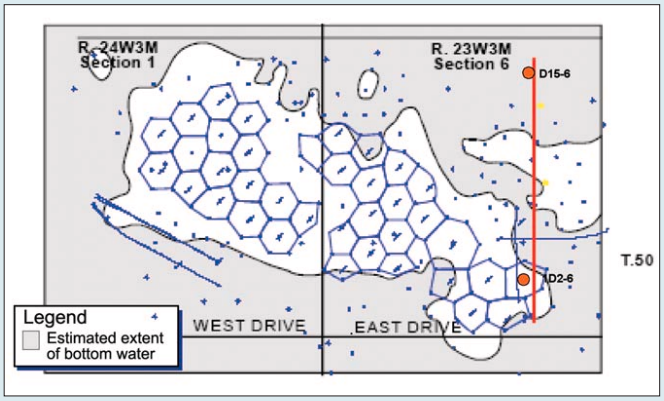

Figure 3. *Map of the time-lapse seismic survey location (red line). The honeycomb shape is a seven-spot steam-drive pattern. Most wells around the seismic line are CCS wells (modified from Wong et al., 2001).*

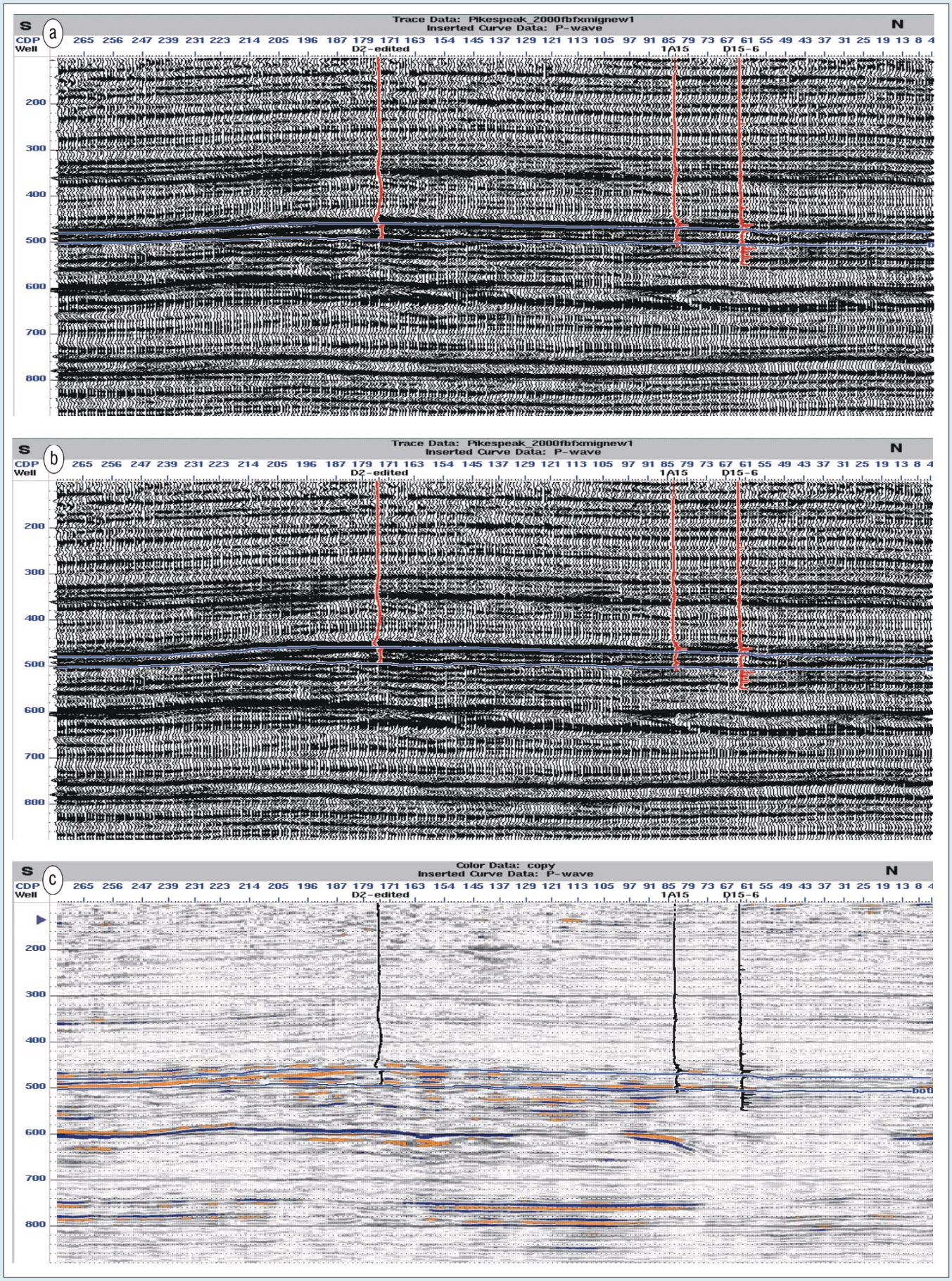

Figure 4. *Final migration stacks with conventional scaling for (a) the 1991 survey, (b) the 2000 survey, and (c) their difference. Orange is positive, and blue is negative.*

Table 3. *Production history for some of the wells in the reservoir simulation. Wells are listed in order from south to north along the seismic line.*

Well name [meters from seismic lines]	Brief history	Status in 1991	Status in 2000
L8 [~60 m]	CSS: 8/1985–10/1988, Prod.: 9/1992–1/1993, Inj.: 2/1993–4/1993, Prod.: 4/1993–2/1997	Shut-in (since 10/1988)	Shut in (since 8/1997)
3B1-6 [~60 m]	CSS: 6/1984–9/1984, Inj.: 11/1990–1/1991, Prod.:1/1991–12/1991, Inj.:9/1992–11/1992, Prod.:11/1992–9/1993, Inj.: 9/1993–12/1993, Prod.:12/1993–10/1999, Inj.:10/1999–11/1999, Prod.: 12/1999–7/2003	Producing (since 1/1991)	Producing (since 12/1999)
1D2-6 [within 10 m]	CSS: 11/1983–12/1986, Inj.: 8/1992–9/1992, Prod.: 9/1992–7/1993, Prod.: 4/1994–9/1994, Prod.: 3/1995–12/1995, Prod.: 5/1996–10/1997, Inj.: 10/1997–1/1998, Prod.: 2/1998–7/2003	Shut-in (since 1/1987)	Producing (since 2/1998)
3C1-6 [~40 m]	CSS: 12/1983–5/1986, Inj.: 8/1992–9/1992, Prod.: 10/1992–7/2003	Shut-in (since 8/1986)	Producing (since 10/1992)
T3 [~20 m]	Inj.: 8/1995–10/1995, Prod.: 10/1995–7/1997, Inj.: 7/1992–9/1997, Prod.: 9/1997–2/1998, Inj.: 2/1998–7/2000	Not drilled	Injection (since 2/1998)
W1 [~60 m]	Inj.: 9/1999–10/1999, Prod.: 10/1999–2/2000, Inj.: 2/2000–1/2001, CSS: 1/2001–7/2003	Not drilled	Injecting (since 2/2000)
V5 [~20 m]	Inj.: 11/1996–12/1996, CSS: 1/1997–8/1998, Prod.: 8/1998–3/2000, Inj.: 3/2000–4/2000, CSS: 3/2000–7/2003	Not drilled	Producing (since 8/1998)
W3 [~60 m]	Inj.: 10/1999–10/1999, Prod.: 10/1999–1/2000, Inj.: 1/2000–2/2000, CSS: 2/2000–7/2003	Not drilled	Producing (since 2/2000)
V10 [~20 m]	Inj.: 5/1997–6/1997, Prod.: 7/1997–3/1998, Inj.: 4/1998–5/1998, Prod.: 5/1998–2/1999, Inj.: 2/1999–3/1999, Prod.: 3/1999–4/2000, CSS: 4/2000–7/2003	Not drilled	Producing (since 3/1999)
D15-6 [~20 m]	Abundant well with logs		
Y1 [100 m]	Inj.: 7/1998–9/1998, Prod., 10/1998–1/2000, Inj., 2/2000–3/2000, CSS: 4/2000–7/2003		

Inj. = injection; Prod. = production; CSS = cyclic steam stimulation

relevant part of Pikes Peak Field were provided by Husky Energy. Laboratory test results by Core Laboratories for the cores from well D2-6 are also available for this study.

Time-lapse seismic processing. The two repeated survey lines used in this study were acquired nine years apart. The first survey (single-component) was acquired in 1991 and was treated as a reference survey here. The second survey (multicomponent) was not designed as a time-lapse study, and the two surveys have different field parameters (Table 1). In addition, the 2000 survey contains more noise due to more production activity compared to the earlier survey and more ground roll due to acquisition geometry changes. Consequently, processing is required to remove the differences due to acquisition geometry, wavelet shape, spectral content, amplitude, and phase differences in an attempt to leave only seismic differences associated with changing reservoir conditions.

The two surveys were processed with the same processing flow: reformat, spherical gain recovery, geometry assignment and trace editing, surface consistent deconvolution, partial spectrum balance, weathering statics and surface consistent statics, NMO and mute application, TRIM statics, amplitude equalization, stacking, spectral balancing, FX predictive decon, finite-difference migration, final bandpass filter, final amplitude equalization (scaling), phase match, and time match. Finally, we derive the difference plot between the two final stacks.

The spherical divergence correction was tested before its application on the data. A surface consistent deconvolution was applied in order to obtain enhanced frequency and amplitude preservation results and to give consistent deconvolution results for gathers with different local features. Spectral balancing was used to suppress anomalously high amplitudes for certain frequencies and balance the amplitude spectra.

Although the two surveys were both acquired in the winter, the weathering layer could be different due to different temperature and environmental conditions; therefore, the weathering statics were calculated separately. To make the two surveys as comparable as possible, we limited the shot and receiver offset to 1200 m, which is the far offset for the 1991 survey. The same mute was applied to both the surveys. Because weathering layer changes could influence deeper events, velocities were picked for each survey individually.

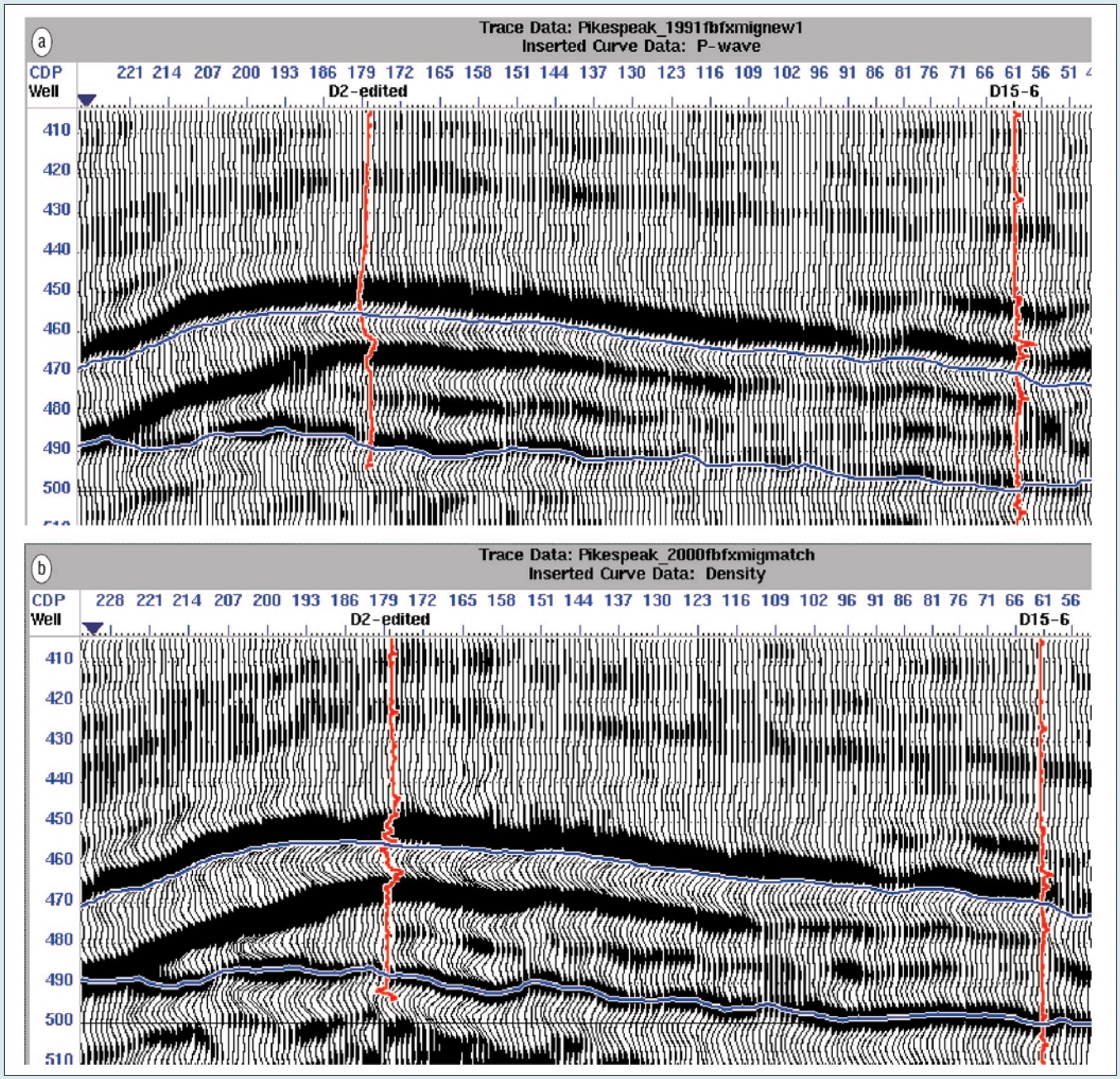

Figure 5. *Enlarged final migrated stack of (a) 1991 survey and (b) 2000 survey.*

Surface-consistent statics and residual statics (TRIM statics) were also calculated individually.

We have to apply scaling to enhance the amplitude in the zone of interest, although scaling can damage relative amplitudes if used without care. We tested three scaling methods and eventually chose conventional scaling using multiple windows at shallow depths to suppress high-amplitude ground roll and one window around the reservoir zone because it appeared to give the results most consistent with the production information. Figure 4 shows the final migration stacks with conventional scaling for the 1991 survey, the 2000 survey, and the 2000 survey minus the 1991 survey. Figure 5 shows an enlargement of the final stacked sections in the area of interest. Changes in the seismic response are evident.

Reservoir simulation results. Reservoir simulation is performed to obtain the change in reservoir pressure, temperature, and fluid saturation, given a production history and a reservoir model. The predicted change in reservoir pressure, temperature, and fluid saturations are then used with the rock physics procedure (discussed in the next section) to calculate the expected seismic response of the reservoir in its predicted state. The predicted change in seismic attributes such as amplitude, impedance, and time delay can then be compared with the observed changes to see if the predicted pressure, temperature, and fluid distributions are consistent with observed changes in the seismic response.

Reservoir simulators are implementations of the laws of conservation of mass, conservation of energy, and energy transport equations. The current model has three physical components: water, oil (dead), and solution gas (methane), and three phases, water, oil, and gas (vapor). The solution gas component can exist in the vapor phase or the oil phase depending on the pressure and temperature. The water component can exist in either the water phase or the vapor phase as steam. Therefore, the gas-phase saturation is composed of both steam and methane. The physical properties of the steam

in the gas phase were considered the same as the methane in the modeling. The dead oil component only exists in the oil phase. Component partitioning between the phases depends on the local pressure and temperature within the reservoir and is calculated using user-specified sets of pressure-volume-temperature (PVT) relationships that depend on the type of oil and gas found in the reservoir. In addition, reservoir properties such as permeability, porosity, thermal heat capacity, and thermal diffusivity must be specified at every location within the reservoir model and constituent relationships must be specified that relate pressure and saturation, capillary pressure, and fluid viscosities to the reservoir conditions. The output of the reservoir simulation consists of pressure, temperature, and fluid saturations for every element, and fluid production at specified time steps. The results presented in this paper were generated using the thermal reservoir simulator. The equations are solved iteratively on a variable 3D reservoir mesh by a finite difference grid and time step algorithm.

In the following, the maximum total production rate and the minimum reservoir pressure were used to model production. The initial model and production history data were provided by Husky, as shown in Figure 6 for one example well. The simulation modeled a region that is 3000 m long. The original model extended 140 m on either side of the two seismic lines and was based on the detailed reservoir interpretation provided by Husky, but it was padded out to 230 m on either side of the seismic lines in order to reduce boundary effects. The grid cells are 20 × 20 m horizontally and vary in thickness. The model consists of three layers corresponding to two interbeded top layers and a lower homogenous sand layer.

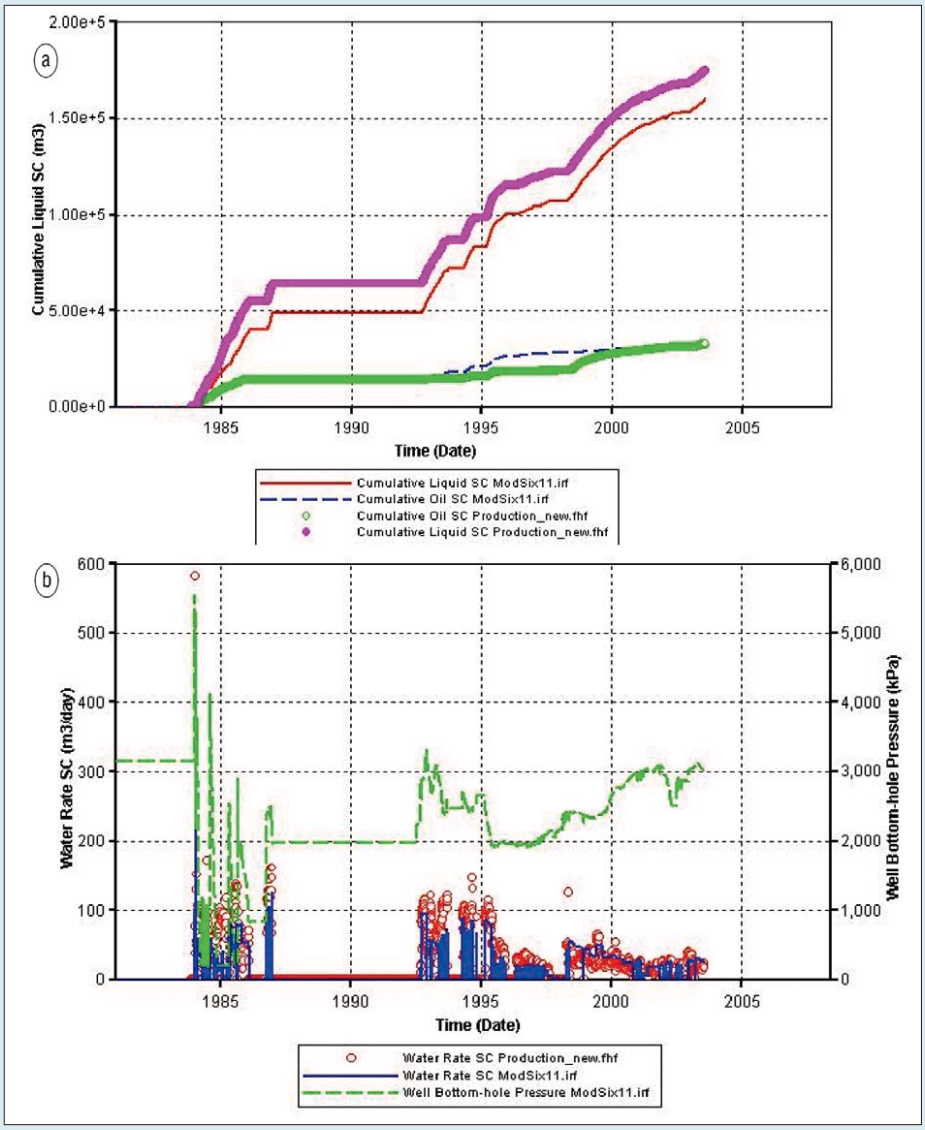

Figure 6. *Reservoir simulation history matching results. (a) Cumulative liquid and cumulative oil production for well 1D2-6 in standard condition. The pink lines are the cumulative liquid productions. The red line is the cumulative liquid production from the simulation output. The green lines are the cumulative oil production. The dashed blue line is the cumulative oil production from the simulation output. (b) Water rate and the bottom-hole pressure for well 1D2-6. The red dots are the water rate in standard condition. The blue line is the water rate in standard condition from the simulation output. The dashed green line is the well bottom-hole pressure from the simulation output (there is no pressure history).*

The response of gas to changes in reservoir conditions plays an important role. In particular, low pressure or high temperature tends to exsolve gas from the oil phase to the vapor phase, and at high pressure and low temperature, gas tends to dissolve into the oil phase. For example, the low pressure during a production period may cause solution gas to vaporize. Additionally, steam injection causes local increases in pressure, temperature, and gas (steam) saturation.

CSS started in the southern part of the reservoir in 1983 at well 1D2-6. The average steam injection duration was 10–30 days followed by a few days of soak, and 5–10 months of production. The reservoir simulation is based on the injection and production history from January 1981 to August 2003. A summary of the production details is found in Table 3.

Once the model was constructed, the horizontal permeability was adjusted until the production history was matched. Production history matching results for a typical well, 1D2-6, are shown in Figure 6. For well 1D2-6, the simulated cumulative liquid production is somewhat lower than the history data (Figure 6a) because simulated bottom hole pressure (BHP) dropped below the minimum BHP constraint of 202 kPa limiting the total production (Figure 6b). The calculated cumulative oil production is a good match to the observed history, but the calculated cumulative water production is somewhat low, explaining the under-prediction of the total production. The BHP history is unavailable for comparison.

The reservoir simulation outputs include the values of reservoir temperature, pressure and water, oil, and gas saturations during the simulation history. Figure 7 shows the 3D distribution of temperature, pressure, and gas saturation, respectively, at the preproduction starting time in 1981, the time of the first seismic survey in February 1991, and the time of the second survey in March 2000. Although the 3D nature of the distributions is clear, the following synthetic modeling is based on the 2D temperature, pressure, and saturation pro-

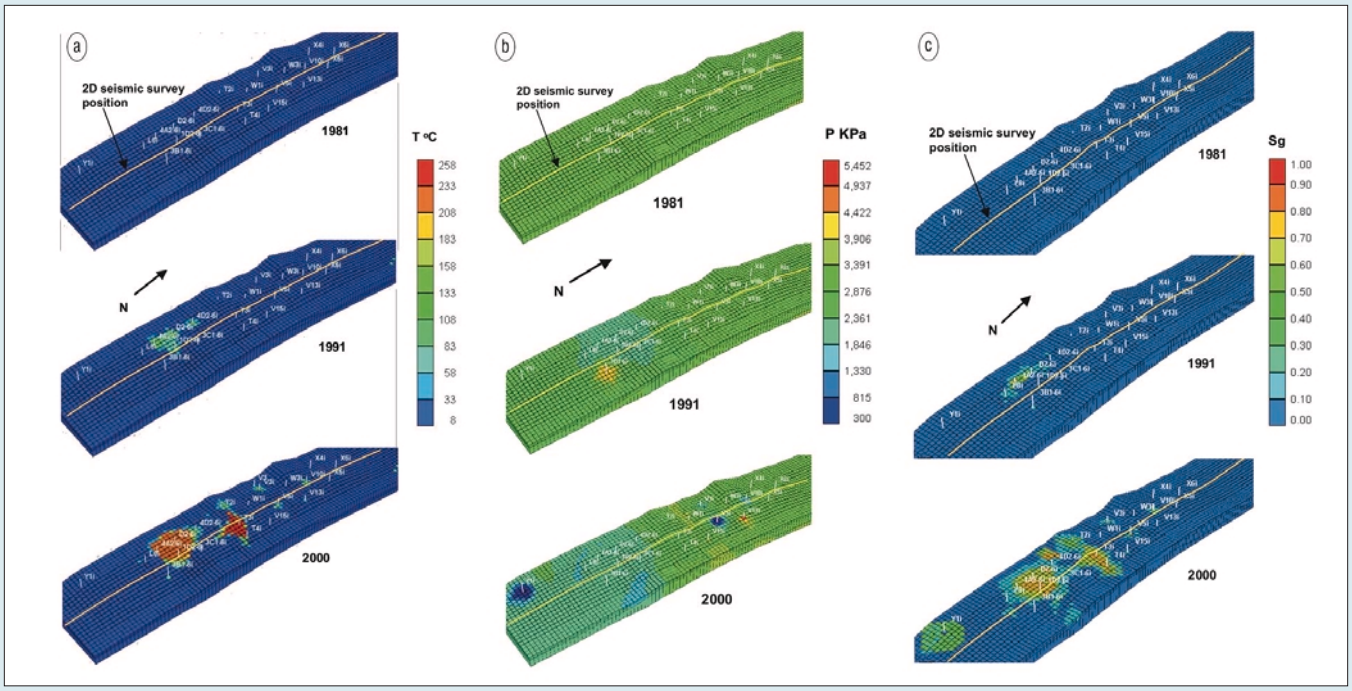

Figure 7. *Simulation results for preproduction (1981), at time of 1991 survey and at time of 2001 survey. (a) Temperature distribution, (b) pressure distribution, and (c) gas saturation distribution.*

file along the trace of the line.

Figure 8 shows the simulated values of pressure, temperature, gas saturation, and oil saturation along the trace of the seismic lines for the preproduction and the 1991 and 2000 survey times. The wells within 60 m of seismic lines were projected to the profile. The distribution of pressure, temperature, and saturation is complex and reflects the production history summarized in Table 3. For example, wells V5 and V10 were not drilled in 1991 and the area around them shows background conditions at that time. By the time of the 2000 survey, the wells had been through several injection and production cycles and they were in the production phase. Consequently, the temperature is elevated above background, the pressure has been lowered due to being in the production phase, the oil saturation has declined, and gas is evident. The gas is not residual steam but has exsolved from the oil phase due to the lowering of pressure. Well T3 also was not drilled in 1991, and CSS started in 1995. At the time of the 2000 survey, the well had been injecting steam since 1998. The high pressure reflects the current injection cycle and the high temperature and low oil saturation reflects the effects of past injection and production. In this case, given the high pressure, the elevated gas saturation is mainly steam as the solution gas would dissolve in the residual oil given the elevated pressure. In contrast, in the older part of the field in the vicinity of wells L8, 1D2-6, and 3B1-6, previous CSS activity has elevated the temperature, reduced the oil saturation, and increased the gas saturation at the time of the 1991 survey. The previous reservoir conditions must be taken into account when interpreting the difference between the 1991 and 2000 surveys.

After analyzing the results, we make the following observations. The net temperature change progresses at about 5–8 m per year (average effect of production and injection). Net pressure responses are much more rapid, on the order of 20 m per month, and changes had reached the boundary elements of the model by the 1991 survey (Figure 7b). The original reservoir had no gas cap, however, the heavy oil has solution gas in it. During steam injection the reservoir temperature, pressure, and gas saturation increased around the injection wells. During production the temperature and pressure decreased. Because pressure spreads rapidly, some locations away from the production well experience low pressure causing solution gas to exsolve from liquid oil. Consequently, the distribution of gas in the reservoir is complicated and not necessarily intuitive, making it difficult to make reservoir state interpretations without the aid of reservoir simulation. Analysis of the following rock physics modeling results shows that the gas distribution is a dominant factor in determining the seismic response and seismic velocity.

Rock physics model. The rock physics procedure, outlined in detail by Zou (2005) is used to relate the reservoir state as calculated by the reservoir simulator to the seismic response. The compressional-wave velocity and shear-wave velocity can be written as

$$V_p = \sqrt{\frac{K_u + \frac{4}{3}\mu}{\rho_u}} \tag{1}$$

$$V_s = \sqrt{\frac{\mu}{\rho_u}} \tag{2}$$

respectively, where K_u is the saturated (undrained) rock bulk modulus, μ is the saturated rock shear modulus, and ρ_u is the saturated rock bulk density. Consequently, we must relate the reservoir state and change in reservoir state to K_u, μ, and ρ_u.

Gassmann's equation has been used successfully in seismic studies to relate the bulk modulus of a saturated rock (K_u) to the dry rock bulk modulus (K_d), the solid grain bulk modulus (K_s), the average fluid bulk modulus (K_f), and the porosity ϕ as follows:

$$K_u = K_d + \frac{(1 - K_d / K_s)^2}{\frac{\phi}{K_f} + \frac{1-\phi}{K_s} - \frac{K_d}{K_s^2}} \tag{3}$$

In addition, the undrained shear (μ) modulus is assumed to be the same as the dry shear modulus and it is assumed unaffected by the properties of the saturating fluid. This

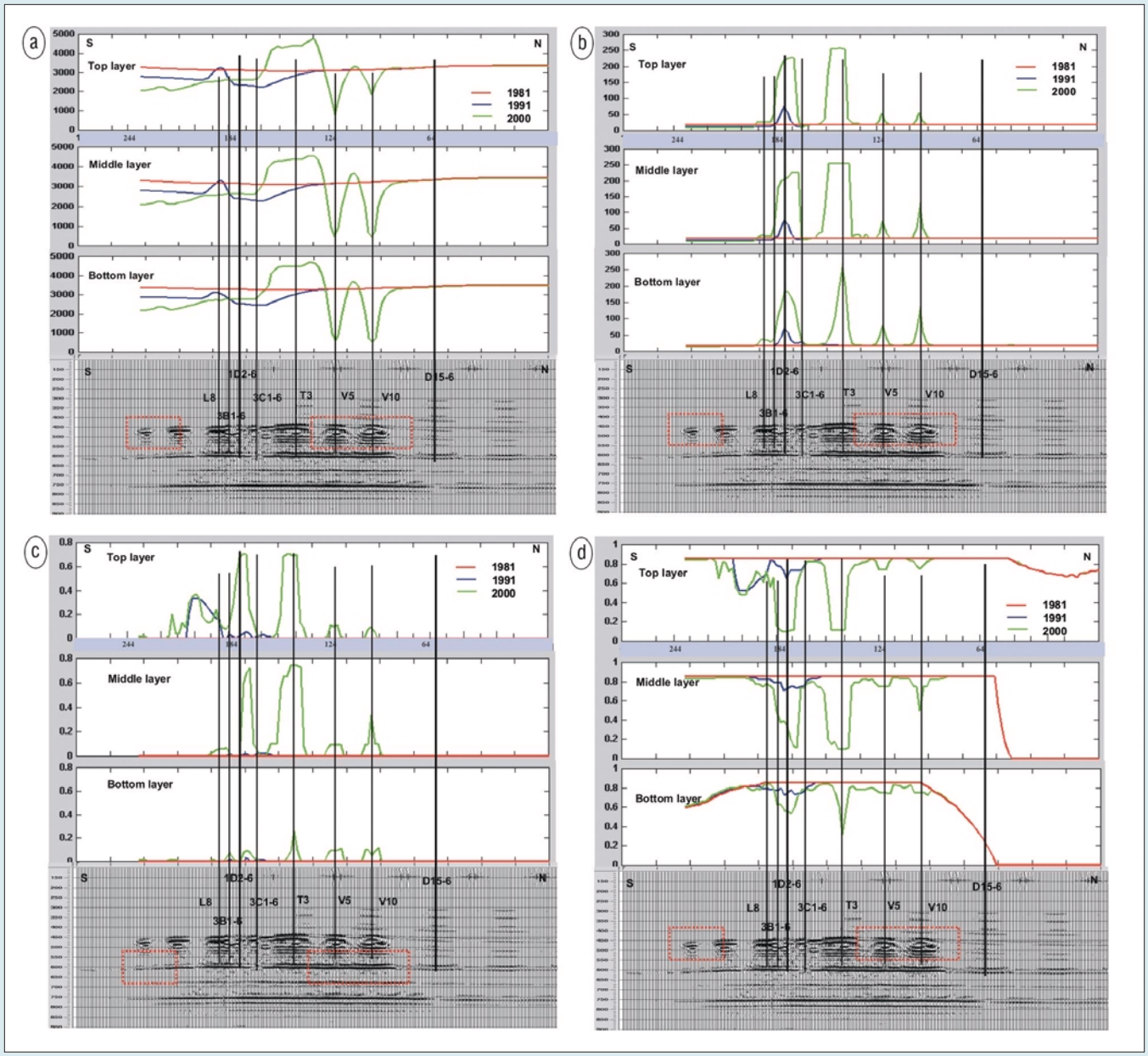

Figure 8. *Reservoir simulation results profiled along the trace of the time-lapse seismic lines. Results are presented for preproduction (red), at the time of the 1991 survey (blue) and at the time of the 2000 survey (green) for the top, middle, and bottom reservoir zones. (a) Reservoir pressure (KPa), (b) reservoir temperature (°C), (c) gas saturation, and (d) oil saturation.*

assumption is generally reasonable for light oil since the viscosity of light oil is relatively low. However, the assumption may not be reasonable for heavy oil because of the higher viscosity. To check this assumption, Zou (2005) used the viscoelastic stress-strain relationship described by Bullen (1963) to show the viscosity effect was negligible for steam injection temperatures. Nevertheless, a rock physics relationship specifically adapted to heavy oil should be the focus of future research efforts.

To use equations 1, 2, and 3, we must specify K_d, K_f, ρ_u, and μ at reservoir conditions as well as K_s and ϕ which are assumed constant. The density of the fluid (ρ_f) and the saturated rock (ρ_u) are obtained from a volume average of the constituents. The estimation of the average fluid bulk modulus (K_f) is determined by using the method proposed by Mavko and Mukerji (1998) who advocate using a value between harmonic and arithmetic means for the bulk moduli of the fluids (gas, oil, and water).

The gas, oil, and water saturation are outputs of the reservoir simulator. The densities ρ_0, ρ_g, and ρ_w, and the fluid bulk moduli K_g, K_o, and K_w at reservoir conditions are calculated using the equations of Batzle and Wang (1992) and parameters derived from cores and logs.

We need to update K_d to account for effective pressure (dP_e) and temperature changes (dT) as the simulation progresses, and this was done using empirical relationships for K_d and μ as a function of temperature and pressure for Pikes Peak Field.

The reservoir simulator calculates the new pressure, temperature, S_g, S_o, and S_w due to reservoir production. Updated values of K_f and ρ_f are calculated as per the method of Mavko and Mukerji (1998). K_d and μ are updated using the emperical relationships mentioned in the previous paragraph. Updated values of K_u are then calculated using the updated values of K_f, K_d, and equation 3. The updated ρ_u is calculated using the updated ρ_f. Finally, the updated values for K_u, μ, and ρ_u are used with equations 1 and 2 to complete the update of

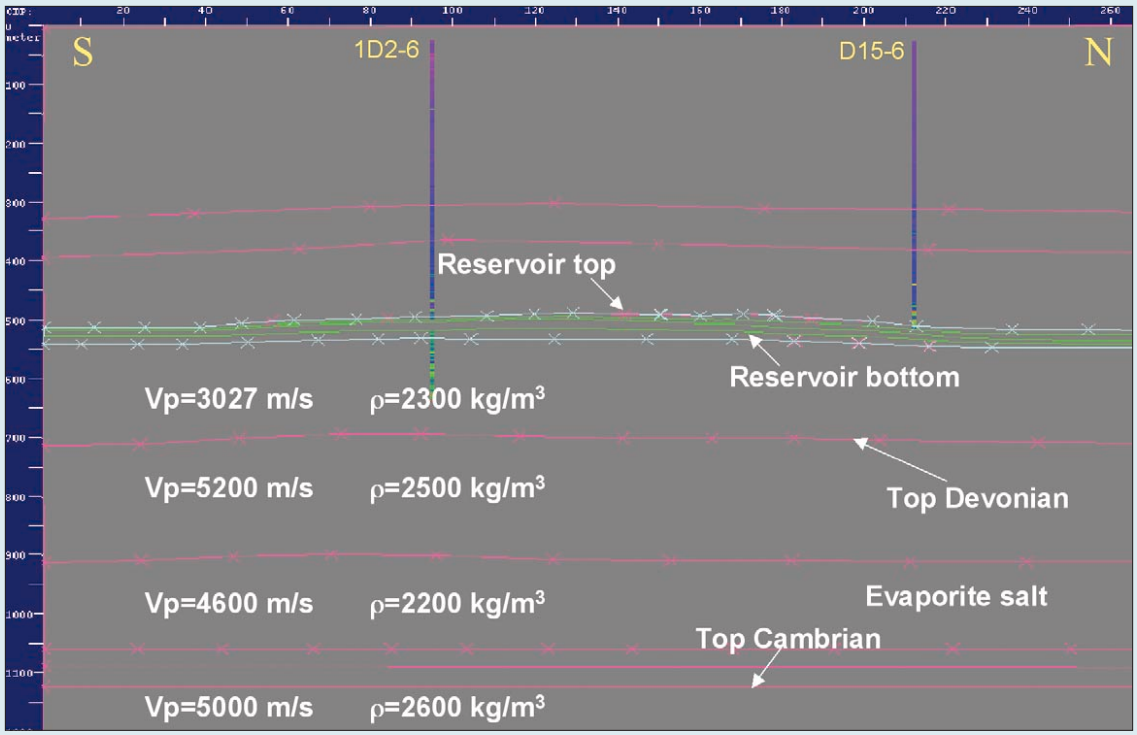

Figure 9. Synthetic seismic model. Above the reservoir velocity and density was interpolated along the structure using well logs at well 1D2-6 and well D15-6, inside the reservoir the values were calculated using the output of reservoir simulation and the rock physics procedure, and below the reservoir we used the average values of well logs from adjacent wells.

seismic properties. The updated seismic properties are then used in the time-lapse seismic modeling described in the next section.

The relationship between the oil reservoir state and the seismic velocity and impedance is complex. For example, as the pressure in the reservoir increases, the effective stress decreases tending to lower the velocity. However, if there is gas present, the higher reservoir pressure will tend to cause the gas to move from the gas phase to the oil phase, tending to increase the velocity. Temperature can also affect the observed seismic velocity. Given the complex distribution of fluids, pressure, and temperature and the many competing factors affecting the seismic response, time-lapse seismic interpretation essentially needs time-lapse seismic modeling in order for us to make meaningful interpretations of results.

Time-lapse seismic modeling. The reservoir simulation has given us a dynamic picture of the reservoir change. To interpret the corresponding seismic response of the reservoir states at two different survey times, we do seismic forward modeling. For the current study, we computed acoustical finite-difference synthetic seismograms using the calculated velocity and density values, as derived from the reservoir simulation.

In time-lapse seismic modeling, we assume that the zone outside of the reservoir zone remains unaffected by production, so the two velocity models have the same velocity outside the reservoir zone, whereas the values inside the reservoir zone can be different to reflect changing reservoir conditions.

The reservoir model grid is 20 × 20 m horizontally, meaning that after applying the rock physics equation, velocity and density values were distributed every 20 m along the seismic line and in variable depths. The values derived from the reservoir model were interpolated onto the 10 m horizontal and 2 m vertical grid of the seismic model profile.

In linking our seismic model to the reservoir, we used both log information and reservoir simulation models. In the seismic model, the velocity values above the reservoir were created using preproduction logs from two wells, D15-6 and 1D2-6 (Figure 9) that were logged in 1978 and 1981. Well D15-6 was an abandoned well in the north part of the reservoir. It never produced; however, the well logs from this well provide a good constraint for our seismic modeling. Therefore, it is marked in all the seismic displays in this paper. First, major horizons that are the reflections of major formations were drawn based on a poststack depth migration section of the 1991 seismic survey. Then, the velocity and density values were interpolated along the horizons. Inside the reservoir, the calculated velocities and densities were derived from the reservoir simulation outputs for the two survey times. The pressure, temperature, fluid saturation from reservoir simulation outputs plus oil and gas gravities, water salinity, K_s (rock grain bulk modulus), K_d (dry rock bulk modulus), μ (shear modulus), and porosity were inputs for the calculation of the velocity and density distributions using the rock physics procedure described earlier. The initial K_d and μ for the reservoir layers are 2.9 GPa and 4.9 GPa respectively. Because we do not have well logs deeper than the Devonian reflector in the Pikes Peak area, we used average velocity and density values from well 10-09 which is about 8 km west of the Pikes Peak area.

To simulate the seismic surveys, we used the same seismic sources and receiver locations as used in the real seismic surveys. The source for the modeling is a 60 Hz zero phase Ricker wavelet. The average velocity in 1991 in the reservoir interval was 2900 m/s, and hence the seismic resolution is around $\lambda/4=V/4f=2900/(4 \times 60)=12$ m. The grid size of the seismic models is 2 m in depth and 10 m horizontally (CDP interval), and they are small enough to ensure the seismic resolution. There are 96 traces in a shot gather, and the shot interval is twice as large as the receiver interval. The modeled time length is 1800 ms which is large enough to ensure that far offset energy was imaged. Normal moveout (NMO) stack and poststack finite-difference migration were performed after the shot gather generation, which was also designed to match the processing for the seismic surveys. The velocities for NMO and migration are converted from the model velocities. The migrated synthetic seismic sections for the 1991 and 2000 survey are displayed in Figure 10.

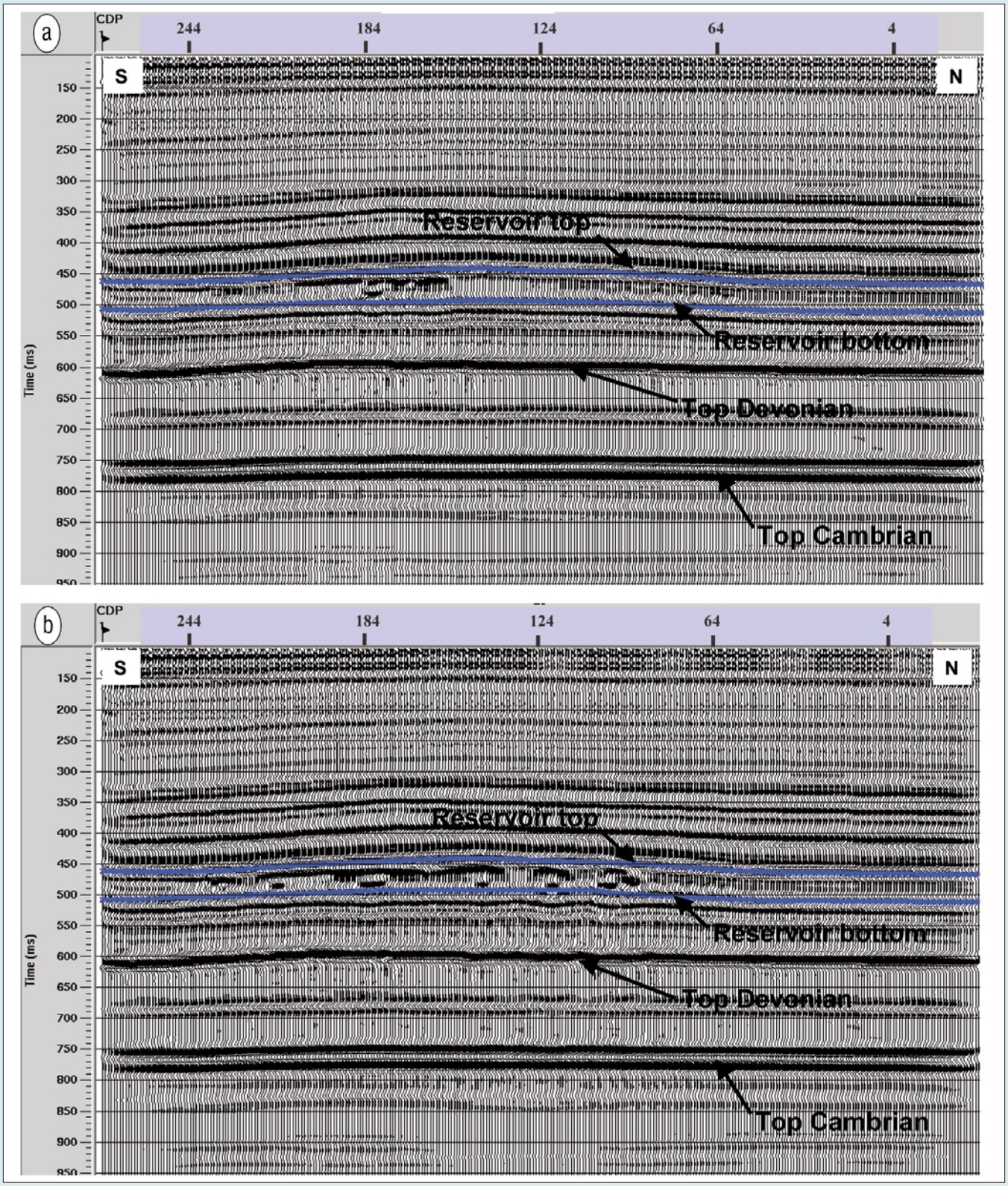

Figure 10. *Migrated synthetic seismic sections for (a) 1991 and (b) 2000.*

From this figure, we can see that the geologic boundaries were correctly imaged. Multiples can be seen on the bottom of the sections, but they are not strong enough to overpower the primaries. The high-amplitude zones inside the reservoir have different features on the two sections. The results can be compared to the observed results in the enlarged sections found in Figure 5. The production-induced amplitude changes can be seen in the lower part of the reservoir. Due to the limitations of the earth model, the shape and the phase of the events in the synthetic sections are not identical to the processed seismic sections. In addition, the seismic modeling was acoustic as opposed to full elastic waveform modeling, so the AVO effects are not properly modeled. Also, we are using 2D modeling, and, as seen in Figure 7, the 3D distribution of fluids, pressure, and temperature may be a confounding issue. Consequently, instead of directly comparing

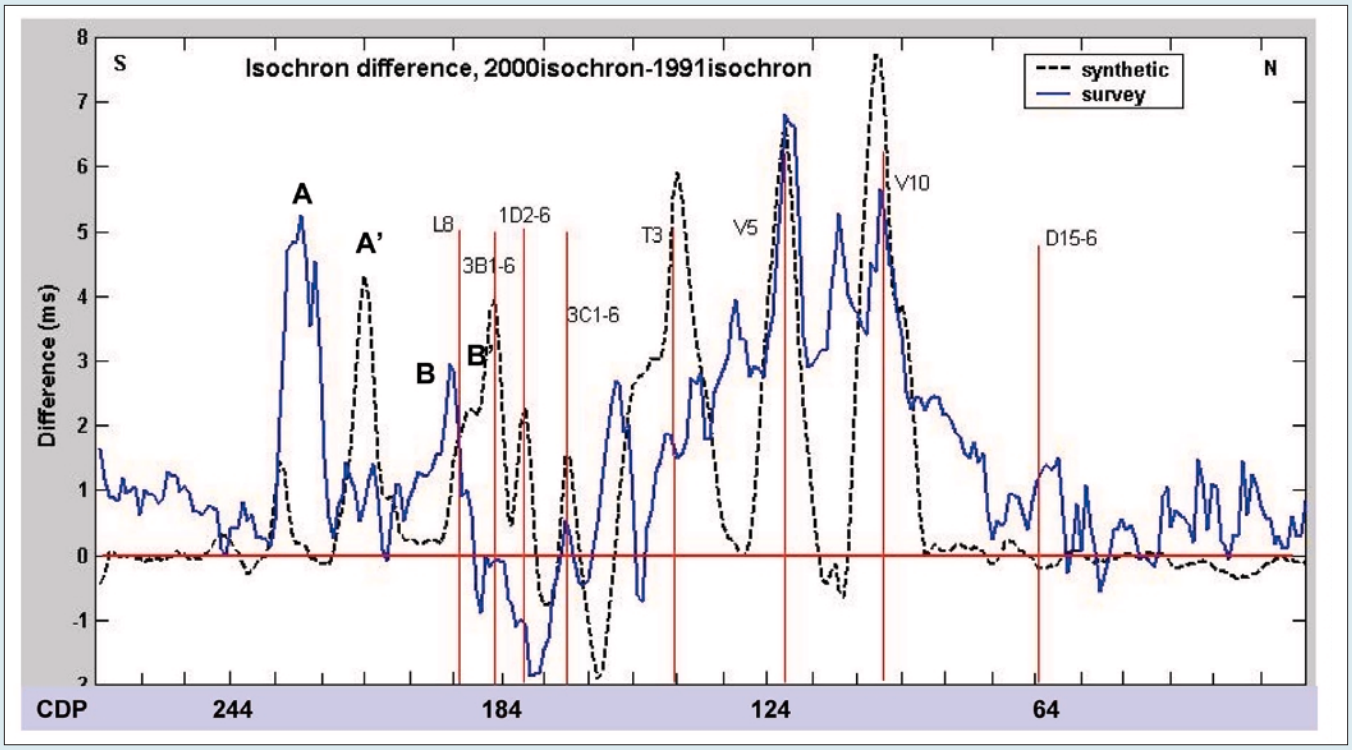

Figure 11. Isochron difference comparison. 2000 survey isochron thickness minus 1991 isochron thickness for seismic (solid line) and simluated profiles.

the images, the interpretation focuses on comparing the character of the changes between the 1991 and 2000 sections of the synthetic and observed seismic sections. Amplitude difference sections were generated by subtracting the 1991 section from the 2000 sections. The synthetic and observed sections show some striking similarities (Figure 12). Difference energy starts in the section at the top of the production zone, and there are strong difference events seen at the top of the Devonian and Cambrian events. In the main, it appears that the reservoir simulation-seismic modeling has captured the character of the seismic changes in the reservoir. However, there are also notable differences in the detail that warrant further scrutiny.

Integrated interpretation. The analysis of many alternative seismic attributes could prove valuable. However, AVO analysis and impedance inversion were found to lead to inconclusive interpretations, most likely due to production noise that contaminated the 2000 survey data. Consequently, we focus on two of the more robust time-lapse difference measures, difference sections and isochron changes. Isochrons were computed by taking the difference in time between the reflection at the top of the reservoir zone and the time of the reflection at the bottom of the reservoir zone. Figure 11 shows the change in isochron values calculated by subtracting the 1991 isochron value from the 2000 isochron value for both the seismic sections and the synthetic sections. The amplitude difference sections for the synthetic profiles and the seismic profiles are shown in Figure 12. Because the gas distribution plays a critical role, the gas saturation profile from the reservoir simulator is also shown in Figure 12.

On the northern end of the line, we see similarities and some differences between the synthetic and field seismic results. Wells V-5 and V-10 appear to produce peaks at nearly identical locations in both the synthetic and the field seismic isochron difference profiles (Figure 11). Strong amplitude differences are seen at the top of the Waseca and at the Cambrian reflection location (Figure 12). The strong reflection difference at the top of the Waseca is due to the increased gas that has exsolved during the production phase. The gas has lowered the velocity and caused an increase in the isochron as well as a time lag accounting for the increased difference energy at the underlying strong Cambrian reflector. However, the location of the isochron difference and the Waseca reflection difference are less distinct in the seismic data than in the simulations, and a strong Devonian energy difference is lacking. One possibility is that the reservoir simulator has not propagated the gas distribution properly. Another possibility is that noise in the seismic data has caused the seismic processing results to smear the response. The reservoir simulator shows no influence from the recently producing wells on this 2D profile and consequently the synthetic seismograms show no influence of the wells. However, small peaks in the seismic isochron difference profiles may be an indication that production is influencing the seismic response, although this is far from clear. Also it is interesting to note the weak difference energy to the north of the production zone. Given that the difference energy is in both the seismic data and the synthetic data, it is probably due to processing artifacts, possibly poststack migration in this complex setting.

The isochron difference section shows a strong peak in the synthetic profile that is lacking in the seismic profile at the location of well T3. However, the amplitude difference sections both show difference energy at the top of the Waseca, Devonian, and Cambrian reflectors, apparently associated with the large gas accumulations from T3 injections. Again, it may be that the gas is more widely dispersed than the flow simulator indicates, or the seismic data has not resolved the details of the gas distribution.

A peak in the isochron difference at the location of 3C1-6 is seen in both the seismic data and synthetic seismograms. The continuity of the energy difference around this location in and below the Waseca is somewhat broken in both the synthetic and seismic profiles. The lessening of the continuity is due to small amounts of gas being present in 1991.

From 3C1-6 on, the seismic response to production appears shifted south compared to the reservoir simulation and simulated response. Such a shift could be due to anisotropy in the permeability field or preferential flow pathways and could have important implications in reservoir management decisions. Peaks A′ and B′ in the synthetic isochron difference profile are possibly correlated with peaks A and B in the seismic isochron difference profile (C and C′ are below or about sample rate, it is hard to say). In addition, there is a boundary of low difference energy south of L8 in the simulated difference section that appears correlated with a similar reduced energy difference in the seismic difference section that is slightly south of the location on the synthetic section. Although this area has seen a lot of production, the reservoir simulation indicates that the gas distribution in 1991 was very similar to the gas distribution in 2000, explaining the lack of difference in the isochrons and seismic amplitude responses. The Devonian and Cambrian reflectors still show difference energy presumably due to the offset traces in the common depth point (CDP) gathers.

At position A′, strong difference energy is seen in the synthetic cross-section as well as a sharp increase in the isochron difference. These are due to the presence of gas in layer 1 in 2000 predicted by the reservoir simulator. There are some similarities in the seismic difference section, but they are not compelling. A major peak, (A in Figure 11), is offset to the south in the seismic isochron difference profile, and it is tempting to correlate it with peak A′ in the synthetic profile. Lower reservoir pressure corresponds to higher effective pressure and higher velocity, however, gas saturation corresponds to lower velocity. This area has both low pressure and small gas saturation. It seems that gas saturation has more impact than low pressure to the seismic response. This area is not located near an active well, but both 1D2-6 and Y1 (Table 3) have been in production for a long time before 2000 survey. The gas has evolved in the model due to the interaction of several wells lowering the pressure to below the bubble point. The gas causes difference energy and a small isochron difference peak at this location in the simulated results. Underlying reflections have not been affected because the gas zone is thin and the time delay increase is small. Consequently, an alternative interpretation for the large peak A in the seismic isochron difference profile is that it reflects a portion of the reservoir whose pressure has decreased below the bubble point. However, the seismic energy difference section lacks evidence to support either of those alternatives.

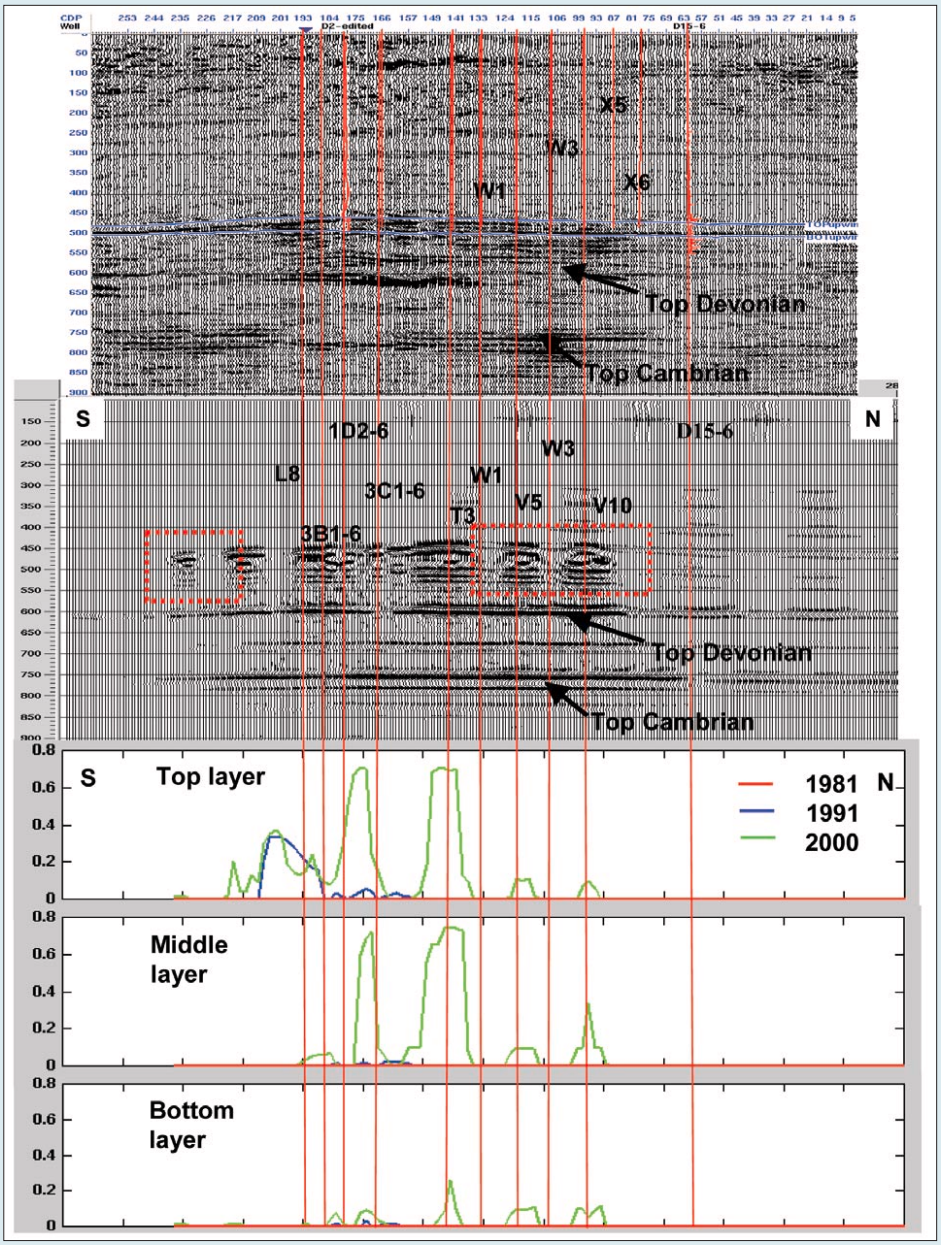

Figure 12. Comparison of seismic amplitude difference profiles and reservoir simulation gas saturation. From top: 2000 seismic amplitude minus 1991 seismic amplitude section, 2000 simulated amplitude minus 1991 simulated amplitude section, simulated gas saturation along trace of seismic profile of top, middle, and bottom layers for preproduction (red), 1991 survey (blue) and 2000 survey (green).

In summary, the synthetic models, the seismic energy difference sections and the isochron difference profiles show similar characteristics. The reservoir simulation and rock physics show that the complex interaction of pressure and steam injection control the gas phase distribution and to a great extent the seismic response changes. However, it should be kept in mind that other factors are at work as well. Increased gas causes increases in the reflection amplitude at the top of the Waseca, time delays to the underlying Devonian and Cambrian formations, and differences in the formation isochrons. These differences are evident on the simulated and field seismic responses. In general the simulated response is more detailed than the seismic response, reflecting either a lack of resolution in the seismic data or an inaccuracy in the reservoir simulation results. The seismic results are consistent in the northern part of the line but seem to indicate that the flow simulator should be adjusted to reflect more

southerly fluid migration.

Conclusions. Many levels of uncertainty exist in the information used to interpret time-lapse data. Ultimately, we wish to arrive at the most probable reservoir conditions and reservoir characteristics such as fluid distribution, preferential pathways, and barriers. The reservoir simulator is the repository for our understanding of the flow dynamics within the reservoir and is used to help make reservoir management decisions. Ultimately, we would like to identify where the reservoir simulator is not performing well so that we can update it. We wish to use the seismic monitoring to evaluate the reservoir simulator performance. On the other hand, the time-lapse seismic results are subject to noise, processing issues, and complex interacting parameters, and we can use the results of the reservoir simulator and forward seismic modeling to help interpret the results of surveys. Ultimately, we want an interpretation that is consistent with the seismic results to within the level of uncertainty and consistent with the physics of flow and transport.

Two time-lapse 2D seismic lines were acquired in February 1991 and March 2000 in the eastern part of the Pikes Peak heavy-oil field. They were acquired over an area that has undergone cyclic steam stimulation production. The reservoir fluid, pressure, and temperature history was modeled with a thermal reservoir simulator. The results of the simulator output were used in conjunction with a rock physics model to develop synthetic seismic responses over the location of the repeated seismic profiles. Synthetic and measured amplitude difference cross-sections and isochron difference profiles were compared. Cyclic steam stimulation may be perhaps the most complex oil recovery process to be analyzed with this innovative approach, as wells are constantly being switched from injection to production and not necessarily in unison, leading to ever-changing seismic responses.

The largest seismic amplitude differences generally correspond to the zones of greatest production activity. Although not the only factor, variation in gas saturation over time leads to the largest seismic differences. The gas phase can be due to injected steam or the evolution of gas due to lowering the reservoir pressure below the bubble point. Thick gas zones correspond with large traveltime delays in the seismic section. The thin gas zones induce changes only in reflectivity and do not have enough time delay to cause strong seismic differences in the deeper regions below the reservoir zone. If the gas zone is present in the first survey as well as the second survey, its presence may not be detected by evaluating differences.

Pressure propagates more rapidly than either temperature or fluids. If the pressure drops below the bubble point, gas can evolve. Gas also can exist as injected steam. Consequently, reservoir simulation is helpful in unraveling the interpretation of time-lapse seismic results in the presence of complex interactions of temperature, pressure, and fluid saturation. In particular, simulation may be required to differentiate the seismic signals of injected steam gas phase and gas exsolved from pressure depletion in CSS. On the other hand, as seen in the southern part of the survey line, time-lapse seismic results can indicate areas in the reservoir simulation that have not captured the correct evolution of the reservoir. Reservoir engineers can then update the reservoir simulator, improving their ability to make reservoir management decisions.

Suggested reading. "Seismic properties of pore fluids" by Batzle and Wang (GEOPHYSICS, 1992). *An introduction to the theory of seismology: 3rd edition* by Bullen (Cambridge, 1963). "Constrained three-parameter AVO inversion and uncertainty analysis" by Downton and Lines (CSEG annual meeting, 2000). "Acquisition and processing of the Pikes Peak 3-C 2D seismic survey" by Hoffe et al. (*CREWES Research Report*, 2000). "Delineation of steam flood using seismic attenuation" by Hedlin et al. (CSEG Annual Meeting, 2001). "Time-lapse monitoring of the Duri steamflood: a pilot and case study" by Jenkins et al. (*TLE*, 1997). "Bounds on low-frequency seismic velocities in partially saturated rocks" by Mavko and Mukerji (GEOPHYSICS, 1998). "Time-lapse seismic programme at Gullfaks: value and the road ahead" by Najjar et al. (*Petrolum Geoscience*, 2003). "Husky's success at the Pikes Peak thermal project" by Sheppard et al. (UNITAR Conference, 1998). "Multicomponent VSP and lake-bottom cable surveys-Pikes Peak, Saskatchewan" by Stewart et al. (*CREWES Research Report*, 2000). "Petroleum geology of Pikes Peak heavy oil field, Waseca Formation, Lower Cretaceous, Saskatchewan" by Van Hulten (Canadian Society of Petroleum Geologists, *Memoir 9*, 1984). "Heavy-oil reservoir characterization using elastic wave properties" by Watson et al. (*TLE*, 2002). "Integrated geological and geophysical analysis of a heavy-oil reservoir at Pikes Peak, Saskatchewan" by Watson (MSc thesis, University of Calgary, 2004). "Meeting the challenge to extend success at the Pikes Peak steam project to areas with bottom water" by Wong et al. (SPE 71630, 2001). "Processing the Pikes Peak walkaway VSP survey and estimating a Q-factor" by Xu (AOSTRA Project, 2001). "Reservoir characterization by combining time-lapse seismic analysis with reservoir simulation" by Zou et al. (CSEG *Recorder*, 2005). "Integration of seismic methods with reservoir simulation, Pikes Peak heavy oil field, Saskatchewan" by Zou (PhD thesis, University of Calgary, 2005). TLE

Acknowledgments: We thank Alberta Oil Sands Technology Research Authority (AOSTRA), Natural Sciences and Engineering Research Council of Canada (NSERC) and CREWES sponsors for financial support. We would also like to thank the Computer Modeling Group (CMG) for the use of the STARS thermal reservoir simulator. We also thank Husky Energy Ltd. for access to data and their reservoir model and in particular thank Don Anderson and Larry Mewhort for their help and advice.

Corresponding author: lrlines@ucalgary.ca